2984 *Biochemistry* **2010,** *49,* 2984–2986
DOI: 10.1021/bi100238r

BIOCHEMISTRY
including biophysical chemistry & molecular biology
Rapid Report

Crystallographic and Single-Crystal Spectral Analysis of the Peroxidase Ferryl Intermediate†

Yergalem T. Meharenna,‡ Tzanko Doukov,§ Huiying Li,‡ S. Michael Soltis,*,§ and Thomas L. Poulos*,‡

‡*Departments of Molecular Biology and Biochemistry, Pharmaceutical Sciences, and Chemistry, University of California, Irvine, California 92697-3900, and* §*Macromolecular Crystallographic Group, The Stanford Synchrotron Radiation Lightsource, SLAC, Stanford University, Stanford, California 94025*

Received February 16, 2010; Revised Manuscript Received March 9, 2010

ABSTRACT: The ferryl [Fe(IV)O] intermediate is important in many heme enzymes, and thus, the precise nature of the Fe(IV)−O bond is critical in understanding enzymatic mechanisms. The 1.40 Å crystal structure of cytochrome *c* peroxidase Compound I has been determined as a function of X-ray dose while the visible spectrum was being monitored. The Fe−O bond increases in length from 1.73 Å in the low-X-ray dose structure to 1.90 Å in the high-dose structure. The low-dose structure correlates well with an Fe(IV)═O bond, while we postulate that the high-dose structure is the cryo-trapped Fe(III)−OH species previously thought to be an Fe(IV)−OH species.

The ferryl, Fe(IV)O, species is a critically important intermediate in a number of metalloproteins and especially heme enzymes. The high redox potential enables Fe(IV)O to serve as a potent oxidant utilized by several heme enzymes, including cytochromes P450, nitric oxide synthase (NOS), cytochrome oxidase, and peroxidases. Since the ferryl intermediate is quite stable in peroxidases, most of what we know about Fe(IV)O in heme enzymes is derived from studies with peroxidases.

In most heme peroxidases, one H_2O_2 oxidizing equivalent is used to oxidize Fe(III) to Fe(IV)O and the second is used to oxidize an organic group to give Fe(IV)O/$R^{\bullet+}$ (*1*), and this activated intermediate is called Compound I. In most heme peroxidases such as horseradish peroxidase (HRP), R is the porphyrin (*2*), although in yeast cytochome *c* peroxidase (CCP) R is the active site Trp191 (*3*). A majority of studies find that the Fe(IV)−O bond is short, somewhat shorter than 1.7 Å, thus indicating an Fe(IV)═O bond as opposed to an Fe(IV)−OH bond (*4*). An empirical formula called Badger's rule relates the calculated Fe−O bond with the calculated vibrational frequency (*5*), and the experimental frequencies and EXAFS bond distances fit very well to these plots (*5*), further supporting an Fe(IV)═O bond. However, a majority of X-ray crystal structures are distinct outliers giving distances closer to 1.8−1.9 Å (*4*, *6*), one exception being the HRP Compound I structure (*7*). These differences are not trivial since the longer bond predicts that the ferryl species should be protonated to give an Fe(IV)−OH species, while the shorter bond gives an Fe(IV)═O species. The chemistry of each of these species is quite different (*8*), and knowing the correct structure is essential if we are to understand details of heme enzyme mechanisms.

A serious problem encountered at high-intensity synchrotron X-ray sources is rapid reduction of metal centers, particularly high-potential metal centers such as Fe(IV). As a result, great care must be taken to minimize reduction and the redox state should be verified during data collection (for example with UV−vis spectroscopy). We recently found that crystals of the CCP N184R mutant diffract unusually well (*9*) and thus might provide an opportunity to obtain a low-X-ray dose Compound I structure at sufficiently high resolution to resolve the discrepancies between crystal structures and solution studies. Here we present single-crystal spectroscopy together with a composite data collection strategy that has allowed the Fe−O bond distance to be measured as a function of X-ray dose.

Figure 1A shows the single-crystal spectrum of CCP Compound I as a function of X-ray dose. Before data collection, the spectrum in the 500−700 nm region is identical to the solution spectrum of Compound I. After extensive X-ray exposure (inset of Figure 1A), the spectrum clearly is no longer that of Compound I nor is this similar to the Fe(III) high-spin solution spectrum of CCP. The nature of this species will be discussed further. Figure 1B shows the estimated percentage of Compound I remaining in the crystal as a function of X-ray exposure as monitored by changes in the visible spectrum. On the basis of this plot, ∼90% of Compound I remains after it receives an estimated X-ray dose of 0.035 MGy [calculations were performed using RADDOSE (*10*)] or just ∼0.1% of the theoretical radiation damage limit for protein crystals, ≈30 MGy (*11*). Therefore, a data collection strategy for obtaining predominantly Compound I was employed using multiple crystals, none of which received more than 0.035 MGy.

Crystallographic data collection was conducted at 65 K on SSRL BL9-2 (∼4×10^{11} photons/s at 13.0 keV). Nearly 100 crystals were mounted and indexed in an automated fashion. Exposures used for indexing were attenuated by 99% and did not significantly contribute to reduction of Compound I. For each crystal, data collection was conducted in 15 separate runs. Run 1 consisted of 5° of data, representing the first 0.035 MGy of X-ray exposure. Then the same 5° of scanning angle was recollected 12 more times, giving runs 2−13 with an increased X-ray dose. In run 14, a full 120° of data was collected to fully reduce the crystal followed by run 15 which again repeated the same 5° representing the highest X-ray dose. The same 15-run data collection protocol was adopted for similarly sized crystals, and the scanning angles were chosen to optimize the completeness of the data. Each composite data set was assembled by merging 5° of data with identical run numbers from 19 crystals. A total of 15 structures at 1.40 Å resolution were refined providing a picture of

†Work at the University of California was supported by National Institutes of Health Grant GM42614 (T.L.P.).
*To whom correspondence should be addressed. T.L.P.: e-mail, poulos@uci.edu; phone, (494) 824-7020; fax, (949) 824-3280.

 Published on Web 03/15/2010

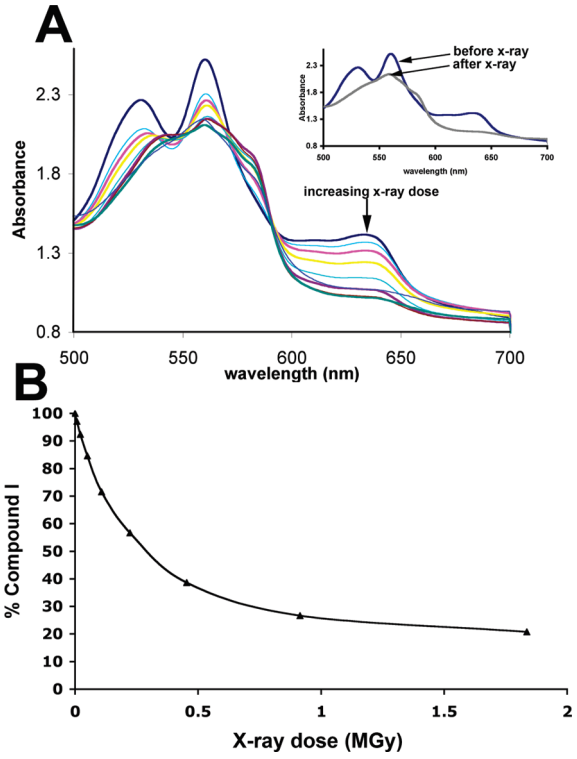

FIGURE 1: Single-crystal spectra of CCP Compound I as a function of X-ray dose. Prior to X-ray exposure, the spectrum is identical to the solution spectrum of Compound I. The estimated percentage of Compound I remaining in the crystal as a function of X-ray dose in panel B was based on the decrease in the absorbance peak at 634 nm.

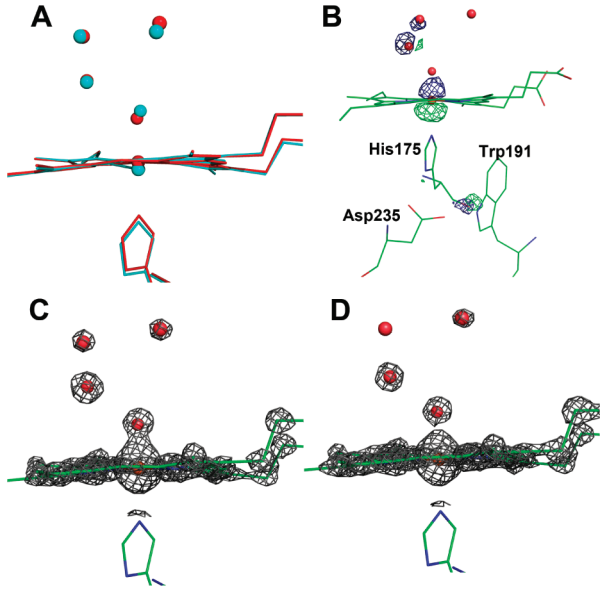

FIGURE 2: (A) Superposition of the low-dose structure (red) on the Fe(III) structure (cyan). Note that the iron is displaced below the plane of the heme in the Fe(III) structure and above the plane of the heme in the low-dose structure. (B) F_o(low dose) − F_o(high dose) electron density difference map using phases obtained from the low-dose structure. The map is contoured at -5.0σ (green) and 5.0σ (blue). (C and D) $2F_o - F_c$ electron density maps contoured at 4.0σ for low-dose data set 1 (C) and high-dose data set 15 (D). Oxygen and water molecules are represented by the small spheres.

the structural changes associated with an increasing X-ray dose (Table S1 of the Supporting Information).

In Figure 2A, we compare the structures of the low-dose (set 1) and the ferric resting state 1.06 Å structure of the N184R mutant (Protein Data Bank entry 3E2O) (*9*). In the ferric resting state, a water molecule is positioned ≈2.0 Å from the heme iron, while in the low-dose data set, the Fe−O oxygen distance is 1.73 Å. In both structures, a water molecule is within H-bonding distance of the Fe-linked oxygen. In the ferric state, the heme iron is displaced from the porphyrin plane by 0.18 Å toward the proximal His ligand, while in Compound I, the iron is displaced by 0.07 Å in the opposite direction toward the distal pocket. Thus, the net movement of the iron is ≈0.25 Å relative to the porphyrin plane because of the oxidation of the iron from Fe(III) to Fe(IV). Note that the water molecules in the distal pocket, including the one closest to the iron, are located in nearly the same position relative to the heme while the His−Fe bond length increases from 2.07 to 2.12 Å upon oxidation to Fe(IV). Thus, the short Fe−O bond in the Compound I structure is due in large part to motion of the iron. As in our previous work on peroxide-treated CCP (*12*), Arg48 in the distal pocket forms a 2.78 Å H-bond with the iron-linked O atom.

We next compare set 1 (low dose, Figure 2C) and set 15 (high dose, Figure 2D) structures. At the 4.0σ contour level, the electron density between the Fe and O atoms is not continuous in set 15 and the Fe−O bond length has increased from 1.73 to 1.90 Å. The local water structure remains largely unchanged. The changes due to X-ray-induced reduction are highlighted by examination of an F_o(low dose) − F_o(high dose) electron density difference map contoured at $\pm 5\sigma$ (Figure 2B). This map clearly shows that the iron is positioned quite differently in each structure and is closer to the distal pocket in the low-dose structure. In addition, the His−Fe bond length decreases from 2.12 to 2.07 Å upon photoreduction again due to the motion of the iron back into the porphyrin plane. The only other notable feature in the F_o(low dose) − F_o(high dose) difference map is around the carbonyl O atom of the heme ligand, His175. This group is slightly less than 0.1 Å closer to Trp191 in the low-dose structure and may reflect a local tightening of the structure around the Trp191 cation radical that provides additional electrostatic stability. The various heme parameter distances are provided in Table S2 of the Supporting Information.

The structures of sets 1−13 next were used to assess how the Fe−O bond changes as a function of X-ray dose, and the results are shown in Figure 3. The fit to a simple straight line equation is remarkably good and extrapolates to zero dose at an Fe−O bond length of 1.72 Å. Raman data (*13*) coupled with Badger's rule (*4*) give an Fe−O bond of 1.68 Å. Therefore, the low-dose Compound I crystal structure agrees within 0.04 Å with the Raman data, and the ferryl center in CCP Compound I can best be described as an Fe(IV)═O species and not an Fe(IV)−OH species.

The nature of the ferryl center after extensive X-ray exposure is intriguing: the short Fe−O bond (1.90 Å) compared to the ≈2.0−2.3 Å bond observed in Fe(III) high-spin peroxidase structures and the total lack of similarity between the high-dose spectrum (Figure 1) and the solution spectrum of Fe(III) CCP show that the high-dose structure is not that of Fe(III) high-spin CCP. The spectrum is similar to that of HRP Fe(II) in both the crystal and solution, except in HRP there is no ligand coordinated to the iron (*7*). Since we clearly see a ligand coordinated to the iron in the high-dose structure, we very likely have trapped either an Fe(II)−OH or Fe(III)−OH species. Unfortunately, we cannot compare single-crystal and solution spectra since formation of the Fe(III)−OH species, and presumably the

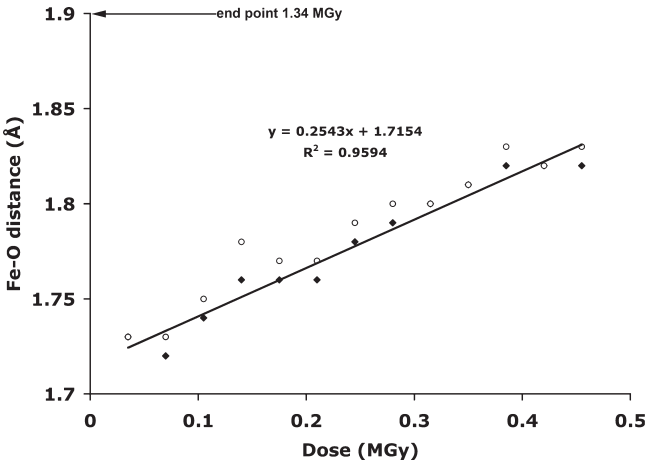

FIGURE 3: Plot of the Fe−O distance as a function of X-ray dose. Each of the 13 structures was refined exactly the same way using the same starting structure and two different protocols. In the first, the distances between the Fe and N atoms [four pyrroles and one His (●)] were restrained, while in the second, no restraints were applied (○). At no time were restraints imposed on the Fe−O distance. The estimated error in the Fe−O bond distance is ≈0.017 Å (see the Supporting Information).

Fe(II)−OH species, requires an increase in pH and CCP is not stable above pH 8.0.

Our first goal in this study was to further develop the necessary methods and protocols required to obtain X-ray structures of high-potential intermediates in metalloproteins. This requires isomorphous crystals that diffract well to have sufficient resolution to obtain the level of accuracy required for estimating subtle bond parameter differences (*7*). Coupling data collection with online single-crystal spectroscopy to monitor the redox state is also essential. Our second goal was to obtain a very low dose X-ray structure of CCP Compound I at high resolution to reconcile the long-standing differences observed in the Fe(IV)−O bond distance between most available X-ray structures and other biophysical techniques. The low-dose CCP Compound I structure agrees within 0.04 Å with previous experimental estimates, indicating that the ferryl species in Compound I is Fe(IV)═O and not Fe(IV)−OH. It should be noted that from the perspective of the heme, CCP Compound I is equivalent to HRP Compound II since both contain Fe(IV) with no porphyrin radical. Thus, it is likely that other crystal structures in which the Fe(IV)−O bond length in Compound II was estimated to be 1.8 Å (*7*, *14*) or longer may also have a significant amount of a reduced iron species.

ACKNOWLEDGMENT

We thank Aina Cohen, John Kovarick, and Michael Hollenbeck for their contribution to the design and implementation of the single-crystal microspectrophotometer. Portions of this research were conducted at the Stanford Synchrotron Radiation Lightsource (SSRL), a national user facility operated by Stanford University on behalf of the U.S. Department of Energy, Office of Basic Energy Sciences. The SSRL Structural Molecular Biology Program is supported by the Department of Energy, Office of Biological and Environmental Research, and by the National Institutes of Health, National Center for Research Resources, Biomedical Technology Program, and the National Institute of General Medical Sciences.

SUPPORTING INFORMATION AVAILABLE

Experimental details and Tables 1S and 2S. This material is available free of charge via the Internet at http://pubs.acs.org.

REFERENCES

1. Poulos, T. L., and Kraut, J. (1980) *J. Biol. Chem. 255*, 8199–8205.
2. Dolphin, D., Forman, A., Borg, D. C., Fajer, J., and Felton, R. H. (1971) *Proc. Natl. Acad. Sci. U.S.A. 68*, 614–618.
3. Sivaraja, M., Goodin, D. B., Smith, M., and Hoffman, B. M. (1989) *Science 245*, 738–740.
4. Behan, R. K., and Green, M. T. (2006) *J. Inorg. Biochem. 100*, 448–459.
5. Green, M. T. (2006) *J. Am. Chem. Soc. 128*, 1902–1906.
6. Hersleth, H. P., Hsiao, Y. W., Ryde, U., Gorbitz, C. H., and Andersson, K. K. (2008) *Chem. Biodiversity 5*, 2067–2089.
7. Berglund, G. I., Carlsson, G. H., Smith, A. T., Szoke, H., Henriksen, A., and Hajdu, J. (2002) *Nature 417*, 463–468.
8. Green, M. T., Dawson, J. H., and Gray, H. B. (2004) *Science 304*, 1653–1656.
9. Meharenna, Y. T., Oertel, P., Bhaskar, B., and Poulos, T. L. (2008) *Biochemistry 47*, 10324–10332.
10. Paithankar, K. S., Owen, R. L., and Garman, E. F. (2009) *J. Synchrotron Radiat. 16*, 152–162.
11. Owen, R. L., Rudino-Pinera, E., and Garman, E. F. (2006) *Proc. Natl. Acad. Sci. U.S.A. 103*, 4912–4917.
12. Bonagura, C. A., Bhaskar, B., Shimizu, H., Li, H., Sundaramoorthy, M., McRee, D., Goodin, D. B., and Poulos, T. L. (2003) *Biochemistry 42*, 5600–5608.
13. Reczek, C. M., Sitter, A. J., and Terner, J. (1989) *J. Mol. Struct. 214*, 27–41.
14. Hersleth, H.-P., Dalhus, B., Görbitz, C., and Andersson, K. (2002) *J. Biol. Inorg. Chem. 7*, 299–304.